DOI: 10.24352/UB.OVGU-2017-010

TECHNISCHE MECHANIK, 36, 1-2, (2016), 57-72
submitted: September 7, 2015

Constitutive Modeling of Additive Manufactured Ti-6Al-4V Cyclic Elastoplastic Behaviour

K. I. Kourousis, D. Agius, C. Wang, A. Subic

Metal additive manufacturing techniques have been increasingly attracting the interest of the aerospace and biomedical industry. A particular focus has been on high value and complexity parts and components, as there the advantages offered by additive manufacturing are very significant for the design and production organisations. Various additive manufacturing techniques have been tested and utilized over the past years, with laser-based technology being among the preferred solutions – e.g. selective laser melting / sintering (SLM / SLS). Fatigue qualification, as one of the primary design challenges to meet, imposes the need for extensive material testing. Moreover, this need is amplified by the fact that currently there is very limited in-service experience and understanding of the distinct mechanical behaviour of additively manufactured metallic materials. To this end, material modelling can serve as a mediator, nevertheless research particular to additively manufactured metals is also quite limited. This work attempts to identify the cyclic elastoplastic behaviour characteristics of SLM manufactured Ti-6Al-4V. A set of uniaxial stress and strain controlled mechanical tests have been conducted on as-built SLM coupons. Phenomena critical for engineering applications and interrelated to fatigue performance (mean stress relaxation, ratcheting) have been examined under the prism of constitutive modeling. Cyclic plasticity models have been successfully employed to simulate the test results. Moreover, a preliminary analysis has been conducted on the differences observed in the elastoplastic behaviour of SLM and conventionally manufactured Ti-6Al-4V and their possible connection to material performance in the high cycle fatigue regime.

1 Introduction

Additive manufacturing of three-dimensional metallic components involves laser assisted depositing and melting of powder metallic materials layer-by-layer, starting from computer aided designs. As additive manufacturing (unlike traditional subtractive manufacturing) is not constrained by geometry or shape, the design paradigm behind additively manufactured components is fundamentally different as it is driven by function (with form following function). This approach offers significant opportunities for light-weighting by identifying key functional features and then organically developing the minimal geometry that will support these functions. Furthermore, this allows for multiple parts to be replaced by a single more complex component by integrating or merging a number of different functions into a single component. To achieve this, we use different computational methods, such as structural and shape optimisation methods based on evolutionary algorithms or topographic optimisation algorithms (Leary et al., 2009; Huang et al., 2012; Leary et al., 2013a; Leary et al., 2013b).
In the past 20 years, additive manufacturing technology has developed from simple three dimensional (3D) printers used to generate non-structural resins into a sophisticated manufacturing process capable to produce objects without the use of tools. Most recently, the focus has been shifted from polymers to metals, primarily aiming to cover the needs of the aerospace, biomedical and automobile industry. Weight reduction of metallic parts using additive manufacturing processes and topographic structural optimisation could go beyond 50% compared to traditional computational and manufacturing methods applied to the same part and material.
High precision manufacturing of Titanium alloys, such as the Ti-6Al-4V, is of primary importance for the biomedical and aerospace industry, due to the high cost involved and the engineering significance of the applications. Various additive manufacturing techniques have been developed, with selective laser melting (SLM) being one of the most commonly used. The SLM process emerged between the late 1980s and early 1990s (Vrancken et al., 2012). The SLM technique uses an infrared fiber laser which assembles solid layers out of loose powder material. In principle, a thin layer of loose powder is initially levelled across a processed platform and selected areas of the powder are melted and consolidated, via a scanning laser beam, in a serial pattern (Simonelli et al., 2012). In comparison with the conventional manufacturing techniques, SLM offers many advantages, such as the reduction of production steps, high level of flexibility, high efficiency in the use of material use and a near

net shape production. However, there are several important effects that need to be avoided: internal stresses development, occurring from steep temperature gradients and high cooling rates during the manufacturing process, and increased porosity. All the effects have an impact on the mechanical behaviour of the material under cyclic loading and low or high cycle fatigue.
Ti-6Al-4V is one of metal alloys employed for SLM produced parts, mainly for applications of high value, performance and complexity, due to its high strength and strength-to-weight ratio. A wide spectrum of mechanical properties over a range of temperatures can be achieved by varying the microstructure of the dual-phase Ti-6Al-4V through appropriate heat treatment and thermomechanical processing (Zhang et al., 2007). However, heat treatment adds time and cost to the production process, reducing partly the advantages offered by additive manufacturing. Moreover, customisation of the microstructure may be achieved through altering the SLM manufacturing parameters. In this case the as-built material can be utilised without further processing or treatment, which is highly preferable from a manufacturing cost point of view. Various researchers have examined the monotonic and high cycle fatigue behaviour of SLM Ti-6Al-4V, nevertheless its elastoplastic response under cyclic loading has not been investigated in much detail, e.g. Leuders et al. (2013). In this context, modelling and simulation of the cyclic elastoplastic behaviour of as-built SLM Ti-6Al-4V is expected to complement the knowledge of researchers and engineers aiming to identify the characteristics of such alloys. This study aims to provide a set of preliminary results from a computational work conducted on the simulation of the cyclic elastoplastic response of as-built SLM Ti-6Al-4V through the implementation of rate independent plasticity models. For this purpose, experimental results are utilised, obtained from an ongoing test campaign conducted at the Centre for Additive Manufacturing of RMIT University.

2 Plasticity Models

Many rate-independent plasticity models for metal material simulation have been developed over the past thirty years. However, only a relatively small fraction of these models enjoy today a wide acceptance by the research community and the industry. Three well established plasticity models (Multicomponent Armstrong-Frederick model, Multicomponent Armstrong-Frederick model with threshold term and Ohno-Wang model) are utilised to model and simulate the behaviour of as-built SLM Ti-6Al-4V. Moreover, a more recently proposed plasticity model (Multicomponent AF with Multiplier) is included in this investigation, in an effort to compare and contrast its performance with this set of widely accepted models.

2.1 Multicomponent Armstrong-Frederick (MAF)

The Multicomponent Armstrong-Frederick (MAF) model is in practice a superposition of a number of Armstrong-Frederick (AF) (Armstrong and Frederick, 1966) back-stress terms (Chaboche et al., 1979). This addition of AF terms, commonly three for most applications, produces a more effective representation of the transient and stabilised stress-strain curves when compared to a model with a single AF term. In practice, each of the different back-stress terms captures the different features of the hysteresis loops. The uniaxial formulation of the MAF model is provided by the following set of equations:

$$a = \sum a_i \text{ , for } i = 1,2,3 \tag{1}$$

Where, a is the total backstress and a_i the added backstresses, each governed by equation:

$$\dot{a}_i = c_i \left(a_i^s - a_i \right) \dot{\varepsilon}^p \tag{2}$$

Dot over quantities shown in equation (2) and elsewhere denotes the time derivative (rate) of backstress a_i and plastic strain $\dot{\varepsilon}^p$. The model material parameters are represented by c_i (backstress evolution pace) and a_i^s (backstress saturation value).

The MAF model has been employed extensively in many applications by both scientists and engineers. It is incorporated as a standard feature in most commercial finite element analysis software (e.g. Abaqus, ANSYS), however it has very limited capabilities in simulating ratcheting effectively. A series of modifications have been proposed to account for this drawback, especially in relation to the improvement of multiaxial ratcheting simulation.

2.2 Multicomponent Armstrong-Frederick with Threshold term (MAF-T)

The ratcheting deficiencies associated with the MAF model were improved with the introduction of a fourth backstress which included a threshold term (Chaboche, 1991). This model is abbreviated as MAF-T (MAF with Threshold term). The threshold stress level, controlled by the corresponding term, signifies a transition point whereby up to it the kinematic hardening rule develops linearly and over that point it evolves according to the original AF rule (nonlinearly). The motivating factor behind the introduction of the threshold term was to reduce the rate of ratcheting predicted by the MAF model by stiffening the loading curve and relaxing the unloading curve. Similarly to the MAF model the total back stress in the MAF-T model is given by the addition of different backstress, as per equation (1). For the uniaxial case, for four backstresses, the following set of equations apply:

$$\dot{a}_i = c_i \left(a_i^s - a_i \right) \dot{\varepsilon}^p \text{, for } i = 1,2,3 \tag{3}$$

$$\dot{a}_i = c_i \left(a_i^s - a_i \left\langle 1 - \frac{\bar{a}_i}{a_i} \right\rangle \right) \dot{\varepsilon}^p \text{, for } i = 4 \tag{4}$$

Where, the model material parameters are represented by c_i (backstress evolution pace), a_i^s (backstress saturation value) and $\bar{a}_i$ (threshold term). The symbol $\langle\ \rangle$ represents the Macaulay brackets.

2.3 Ohno-Wang (O-W)

The Ohno-Wang (O-W) model (Ohno and Wang, 1993a; Ohno and Wang, 1993b) originally acted as a multilinear model, unlike to the MAF and MAF-T models, which predicted no uniaxial ratcheting. In order to overcome this issue a multiplier was added to the dynamic recovery term of the AF backstress, which introduced a slight nonlinearity to each of the defined backstress equations. The uniaxial formulation of the O-W model is as follows [again, for four added backstress terms, as per equation (1)]:

$$\dot{a}_i = c_i \left(a_i^s - a_i \right) \dot{\varepsilon}^p \text{, for } i = 1,2,3 \tag{5}$$

$$\dot{a}_i = c_i \left[a_i^s - a_i \left(\frac{a_i}{a_i^s} \right)^m \right] \dot{\varepsilon}^p \text{, for } i = 4 \tag{6}$$

Where, the model material parameters are represented by c_i (backstress evolution pace), a_i^s (backstress saturation value) and m (multiplier). The multiplier is calculated with reference to ratcheting or mean stress relaxation data. As shown by Bari and Hassan (2000) for small values of m, the higher the predicted ratcheting rate is.

2.4 Multicomponent AF with Multiplier (MAFM)

The Multicomponent AF with Multiplier (MAFM) model was introduced as an improved alternative to the MAF-T model (Dafalias et al., 2008). As a consequence of the incorporation of the threshold term in the original MAF model, an un-physical linear portion of the hysteresis loop was formed. However, the MAFM model is able to improve this issue without affecting the ratcheting simulation accuracy (Dafalias et al., 2008). This was achieved with the introduction of a multiplier term into one of the AF backstresses. The multiplier is used to adjust the rate at which saturation of the backstress occurs, without affecting the saturation level. This operation is analogous to the MAF-T model's threshold term, without the need to check the exceedance of a threshold (which is a computationally expensive task). The uniaxial formulation of MAFM model, for four backstresses [obeying to an additive decomposition, as per equation (1)], is given by the following set of equations:

$$\dot{a}_i = c_i \left(a_i^s - a_i \right) \dot{\varepsilon}^p \text{, for } i = 1,2,3 \tag{7}$$

$$\dot{a}_i = \left[c_i + c_i^* \left(a_i^{*s} - a_i^* \right) \right] \left(a_i^s - a_i \right) \dot{\varepsilon}^p \text{, for } i = 4 \tag{8}$$

With a_4^* (dimensionless multiplier) given by:

$$\dot{a}_4^* = c_4^* \left(a_4^{*s} - a_4^* \right) \dot{\varepsilon}^p \tag{9}$$

Where, the model material parameters are represented by c_i (backstress evolution pace), a_i^s (backstress saturation value), c_4^* (a_4^* multiplier backstresess evolution pace) and a_4^{*s} (a_4^* multiplier backstress saturation value).

2.5 Isotropic Hardening

A nonlinear isotropic hardening rule was also incorporated along each of the kinematic hardening models examined. This addition was deemed necessary for the effective simulation of the strong cyclic softening characteristics of the material under study (Ti-6Al-4V). The governing equation (in uniaxial stress space) for the yield stress (k) is provided below:

$$\dot{k} = c_k \left(k^s - k \right) \left| \dot{\varepsilon}^p \right| \tag{10}$$

Where, c_k the parameter controlling the evolution pace and k^s the saturation value of the yield stress (k).

3 Experimental Data

The experimental data utilised for the purposes of this computational study were obtained from mechanical tests previously conducted at the RMIT University Centre for Advanced Manufacturing. These test data come from tests performed on cylindrical cross section specimens of as-built SLM Ti-6Al-4V material manufactured with an SLM Solutions SLM® 250 HL machine. This manufacturing equipment has a rated power of 400 W under continuous laser mode and a minimal laser spot size of 80 microns. The specimens have been fabricated with a laser power of 175 W, at a laser scanning speed of 710 mm/s, 120μm hatch spacing and a 30μm powder layer thickness. The platform was preheated to 200°C prior to the building process and each specimen had a total of 2,746 built layers.

The microstructure of the obtained specimens was examined with the use of optical microscopy (Phaiboonworachat, 2014). Ti-6Al-4V alloys are composed of two phases, the α-phase (Hexagonal Close Packed, HCP structure) and the β-phase (Body Centered Cubic, BCC), while a α+β phase can be present simultaneously. The examined SLM specimens' samples revealed the presence of a martensitic microstructure (α'-phase). In particular, the characteristic needle shaped thin lamellas (lath martensite) of the α'-phase have been observed (Figure 1a). Moreover, prior β-phase acicular shaped columns, with random orientation, have been identified on the SLM material surface (Figure 1b). The length of the prior β-phase column has been measured as 183.8μm.

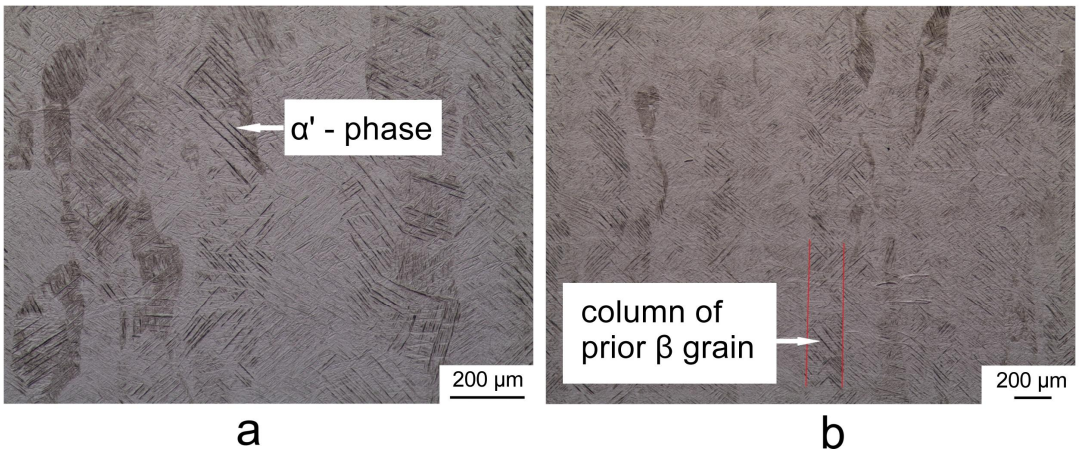

Figure 1. SLM Ti-6Al-4V microstructure micrographs presenting (a) needle shaped thin lamellas α'-phase and (b) characteristic β-phase acicular shaped columns.

A comparison of the microstructure of the SLM material to a wrought material was also conducted. Unlike to the needle shaped lamellas observed in the SLM material (Figure 2a), the wrought material is dominated by a spheroidite microstructure containing α-phase and β-phase (bright areas and dark sports respectively, shown in Figure 2b).

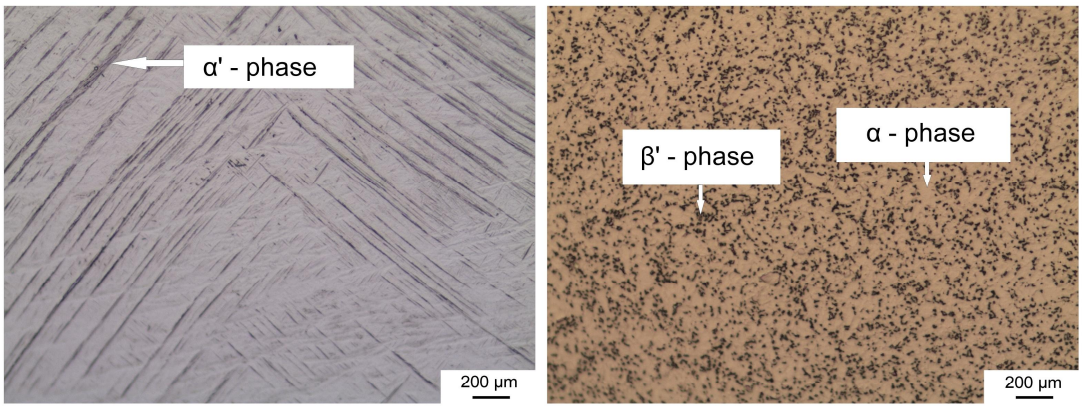

Figure 2. Comparison of the microstructure of (a) SLM Ti-6Al-4V and (b) wrought Ti-6Al-4V.

The specimens were tested under strain and stress controlled loading histories, summarised in the Table 1 and Table 2 correspondingly. The test control (input) parameters for both loading histories are the following:

- Strain Controlled Tests: Symmetric (zero mean strain) cycling at different strain amplitudes (ε_a) for a given number of cycles (150 cycles or lower, where the specimen experienced a failure) (Table 1);
- Stress Controlled Tests: Non-symmetric cycling under different combinations of mean stress (σ_m) and stress amplitude (σ_a) pairs, until specimen failure (Table 2).

Loading History	**Strain Amplitude ε_a**	**Number of Cycles**
Test 1	±1.0%	150
Test 2	±1.5%	150
Test 3	±2.0%	150
Test 4	±2.5%	88* *specimen failure

Table 1. Strain controlled loading histories.

Loading History	Stress Amplitude σ_a	Mean Stress σ_m	Minimum, Maximum Stress $(\sigma_{\min}, \sigma_{\max})$
Test 1	865 MPa	15 MPa	(-850, +880) MPa
Test 2		35 MPa	(-830, +900) MPa
Test 3	875 MPa	30 MPa	(-845, +905) MPa
Test 4		40 MPa	(-835, +915) MPa

Table 2. Stress controlled loading histories.

The test data (results) are not presented independently in this section but in conjunction with the obtained simulation results in the next sections of this paper. However, some important observations are highlighted here, as these are relevant to the objective and focus of this study. In particular, the cyclic tests performed on the as-built SLM material, resulting in elastoplastic behaviour, signify important features related to the fatigue performance of such materials. Figure 3 presents the hysteresis loops obtained from the as-built SLM Ti-6Al-4V strain controlled tests in comparison with previously published experimental data (Mayeur et al., 2008).

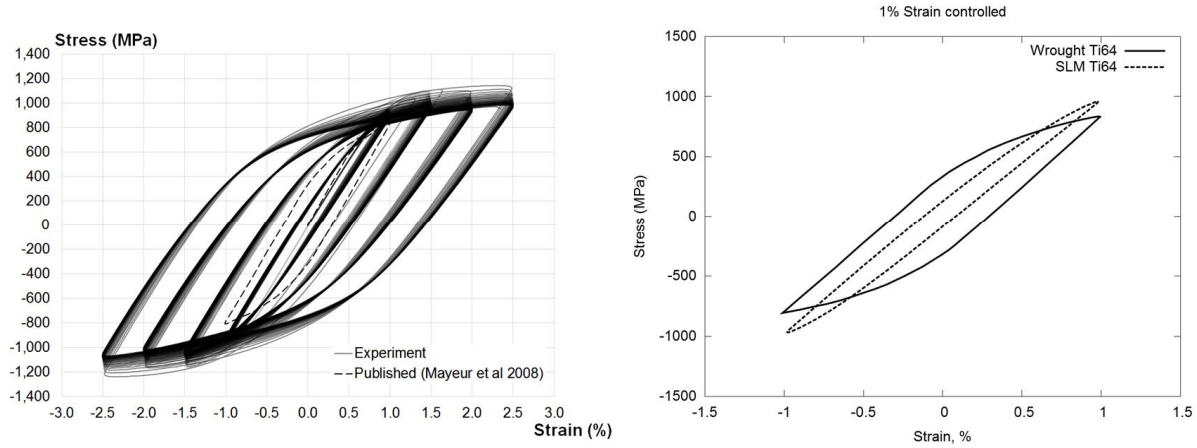

Figure 3. Stress – strain hysteresis loops obtained from the strain controlled testing of as-built SLM Ti-6Al-4V at different strain levels (represented by the solid line) compared to previously published test data for wrought Ti-6Al-4V (Mayeur et al., 2008).

By examining Figure 3 it is noticed that the SLM material exhibits, for each of the four strain levels, a strong cyclic softening behaviour. Moreover, the yield stress, ranging from approximately 917 MPa to 1,096 MPa, is achieved at relatively low strains. This causes a compression in the shape of the hysteresis loops, which is consistent with the brittle nature of the as-built SLM material and its low capacity to undertake plastic deformation during cyclic loading (low plastic deformation dissipation). This particular feature of the studied SLM material is evident in the hysteresis loops corresponding to ±1% strain level, as compared to experimental results for wrought Ti-6Al-4V, obtained from the literature (Mayeur et al., 2008), both shown in Figure 3. It is also noticed that the as-built SLM material exhibits a higher load capacity at the expense of reduced ductility. In summary, one may conclude that:

- High strength and low ductility under cyclic loading are the primary characteristics observed, which are opposed to lower values applicable for wrought Ti-6Al-4V;
- Cyclic softening behaviour observed at all strain levels is also of notice;
- Plastic deformation dissipation, approximated by the area enclosed by the hysteresis loops, is lower for the SLM Ti-6Al-4V as compared to wrought alloy. This, in turn, is believed to have a negative effect on the low and high cycle fatigue life of the materials, as previously reported by Leuders et al. (2013) and Xu et al. (2015).

4 Numerical Implementation

Each of the plasticity models, namely MAF, MAF-T, O-W and MAFM, was implemented numerically in Matlab. The model parameters were obtained with the use of the applicable (for each model) methodology and consequently optimised through a manual iterative fine-tuning process. In particular, the process outlined in Bari and Hassan (2000) and Dafalias et al. (2008) was used to determine the material parameters. The values for the c_i and a_i^s parameters were calculated with reference to the stabilised cyclic stress-strain curve, while the parameters which control the ratcheting rate ($\overline{a}_4$, c_4^*, a_4^{*s} and m) were determined with reference to ratcheting data. Adjustment of these parameters was made until the models could capture sufficiently the amount of ratcheting for a particular load case. It was important that such parameter adjustment was double-checked against the stabilised cyclic stress-strain response to ensure the simulation of the stabilised stress-strain curve was not compromised. The isotropic hardening values (c_k, k^s) were estimated by fitting the uniaxial integrated isotropic hardening equation to stress range versus accumulated plastic strain data in order to define the relationship between these two measures. The final set of material parameters obtained through the aforementioned process, summarised in Table 3, was utilised for the simulation of the experimental results.

		MAF	**MAF-T**	**O-W**	**MAFM**
Initial yield stress (σ_Y)		490 MPa			
Elasticity Modulus (E)		101 GPa			
Backstress	**Model Parameter**				
a_1	a_1^s	105.00 MPa	122.50 MPa	38.96 MPa	122.50 MPa
	c_1	400	400	1,540	400
a_2	a_2^s	69.52 MPa	79.52 MPa	74.74 MPa	79.52 MPa
	c_2	300	300	553	300
a_3	a_3^s	242.10 MPa	140.65 MPa	21.40 MPa	140.65 MPa
	c_3	69	69	100	9
a_4	a_4^s		295.7 MPa	153.85 MPa	9.57 MPa
	c_4		10	26	100
	$\overline{a}_4$		15		
	a_4^{*s}				15
	c_4^*				1,700
	m			0.10	
Isotropic hardening parameters	c_k	2			
	k^s	180 Mpa			

Table 3. Material parameters for plasticity models (MAF, MAF-T, O-W and MAFM)

5 Results

The simulation results obtained for the different models are compared against test data for each of the different loading histories (strain / stress controlled) shown in Table 1 and Table 2. These are presented and discussed in detail in the following sections.

5.1 Strain Controlled Results

The stabilised hysteresis loops at each strain level (1.0%, 1.5%, 2.0% and 2.5%) are presented in Figure 4.It is observed that all models are capable to capture effectively the shape and characteristics of the loops.

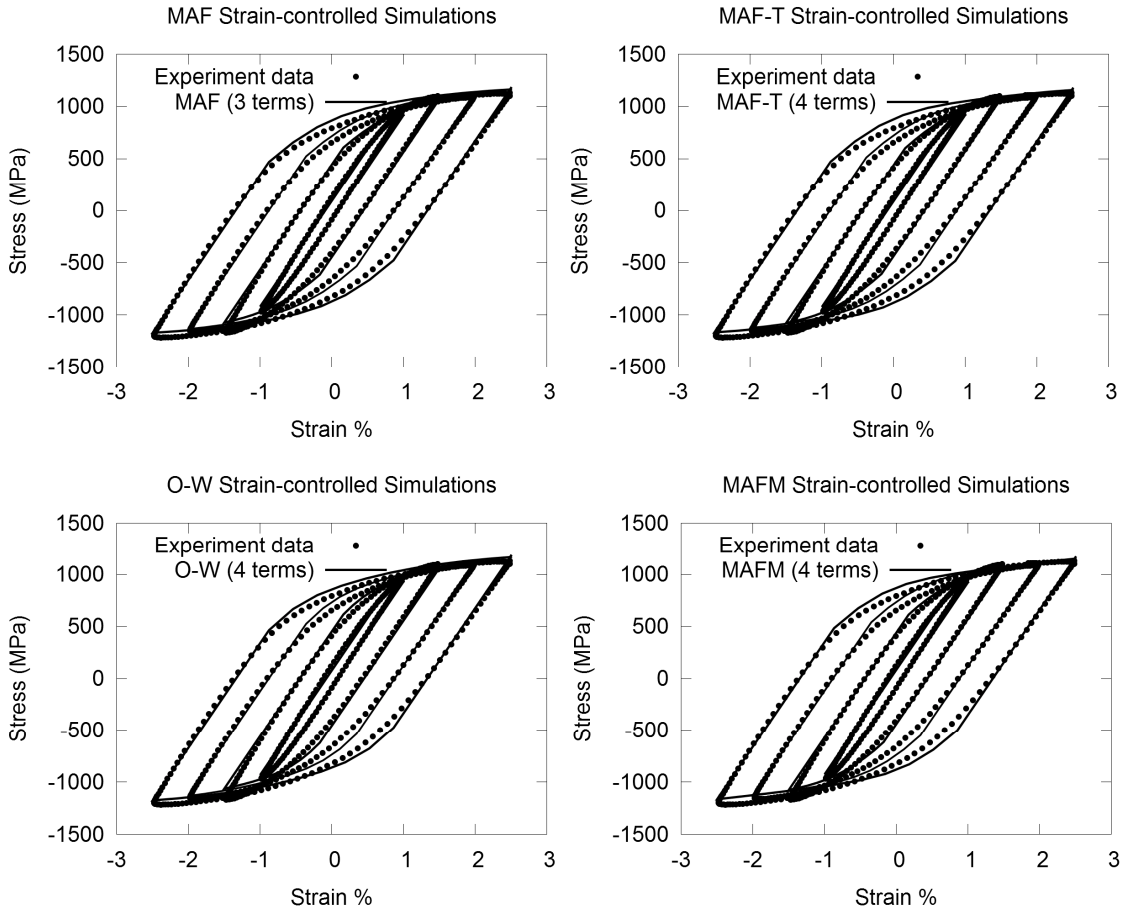

Figure 4. Hysteresis loops obtained from the strain controlled tests, under different strain levels, in comparison with computational results for the MAF, MAF-T, O-W and MAFM models.

A closer look at the cyclic hardening behaviour of the material was considered of interest. This was performed through the calculation of the cyclic hardening factor (H) at different strain levels. The cyclic hardening factor (H) is given by the following equation:

$$\mathrm{H} = \frac{\sigma_{sat} - \sigma_0}{\sigma_0} \tag{11}$$

Where, where σ_{sat} the stress amplitude is in the first cycle and σ_0 is the stress amplitude of any number of cycles.

The results (experimental and computational) are presented in Figure 5. All models perform fairly acceptable. However, one may note that the last point of the experimental curve (corresponding to 2.5% strain) was not captured by any model. This was attributed to the fact that this point corresponds to the prematurely failed specimen (at 88 cycles), which did not allow the cyclic phenomenon evolve fully (no stabilisation occurred).

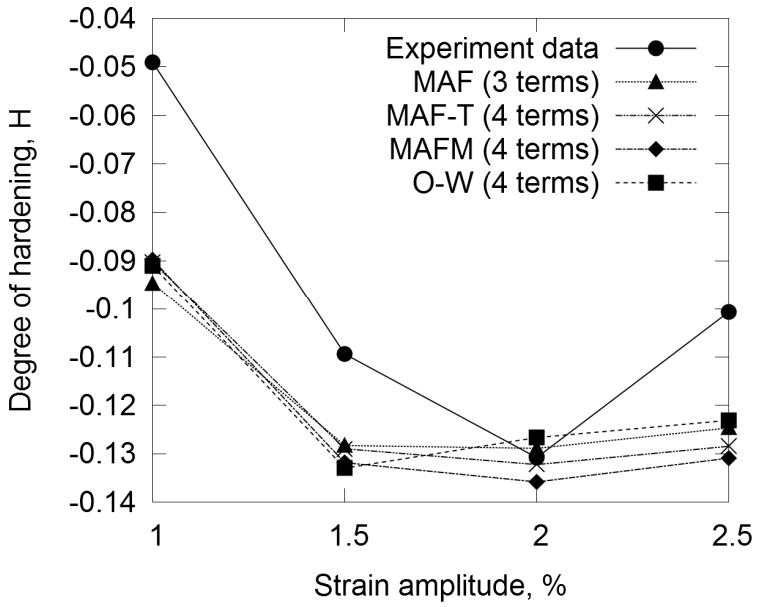

Figure 5. Cyclic Hardening Factor at different strain levels. Comparison of experimental versus computational results for different models.

The material mean stress relaxation was also investigated. For this purpose, the stress amplitude variation was plotted against the number of cycles until saturation, both for experimental and computational results. Figure 6 presents the obtained results for each of the different strain levels and for all models compared. One may note that the models perform better at higher strain levels (2.0% and 2.5%), capturing quite well the experimental curves. All models have similar behaviour in terms of curve fitting, however a closer look at each model's performance is discussed in greater detail in the sequel.

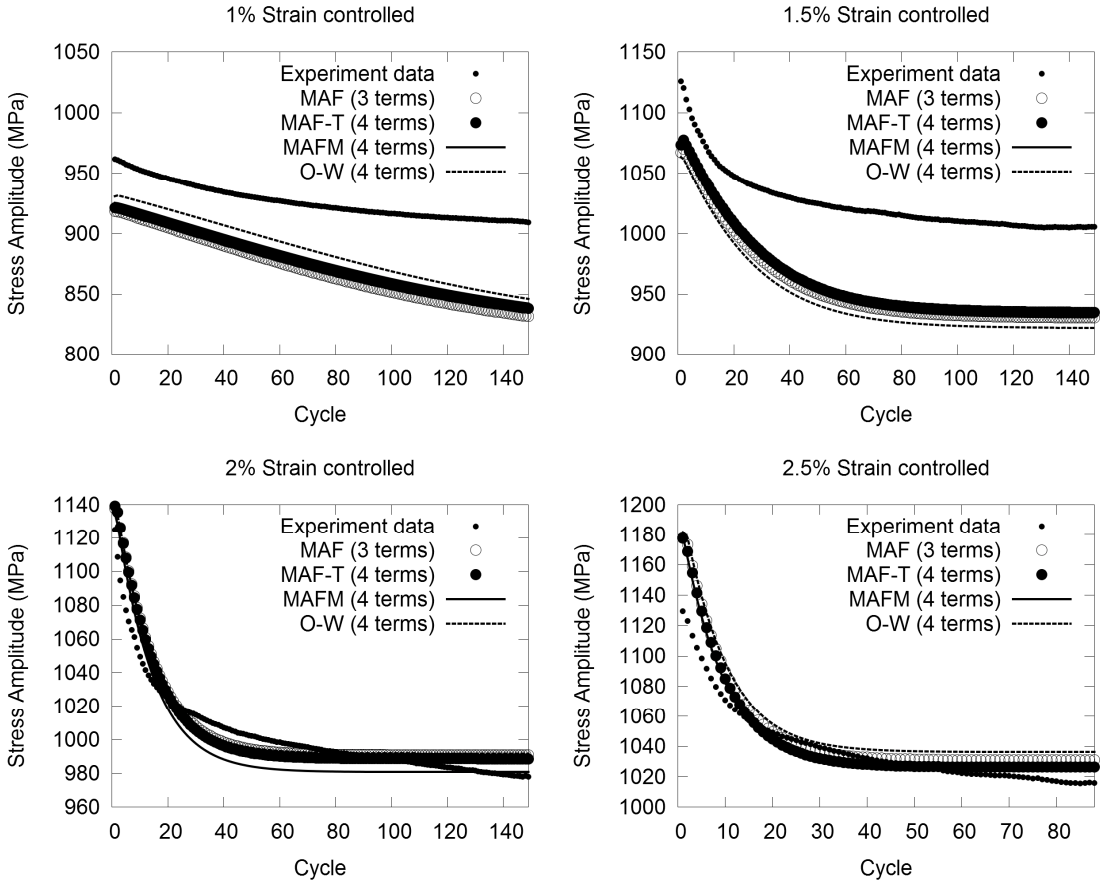

Figure 6. Cyclic Mean Stress Relaxation at different strain levels. Computational versus experimental results for all models in comparison.

An interesting analysis, from the point of view of material fatigue performance, has been attempted via the calculation of the plastic deformation energy dissipation. The capacity of the SLM material to absorb plastic energy was considered important for the completeness of this study, since no such results have been reported in the past, to the best knowledge of the authors. To this end, the plastic energy density (corresponding to the hysteresis loop area) was plotted against the number of cycles, both for test and simulated data. Figure 7 presents these results, while Figure 8 presents the percentile error (%error) between test and simulated data for each model compared. A variation between models, in terms of their capability to capture the test data, is quite evident from these results. This observation provides a useful way to assess more accurately and perhaps in a more representative way, the plasticity models' performance in reference to fatigue behaviour. However, an overall comparison of the models is necessary. This needed to be put under the prism of capturing the various test cases (strain and stress controlled) and characteristic response resulting from each loading cases. For this purpose, a ranking scheme is proposed as a simple way to obtain quantitative results on the overall performance of the models. This scheme is presented in the sequel.

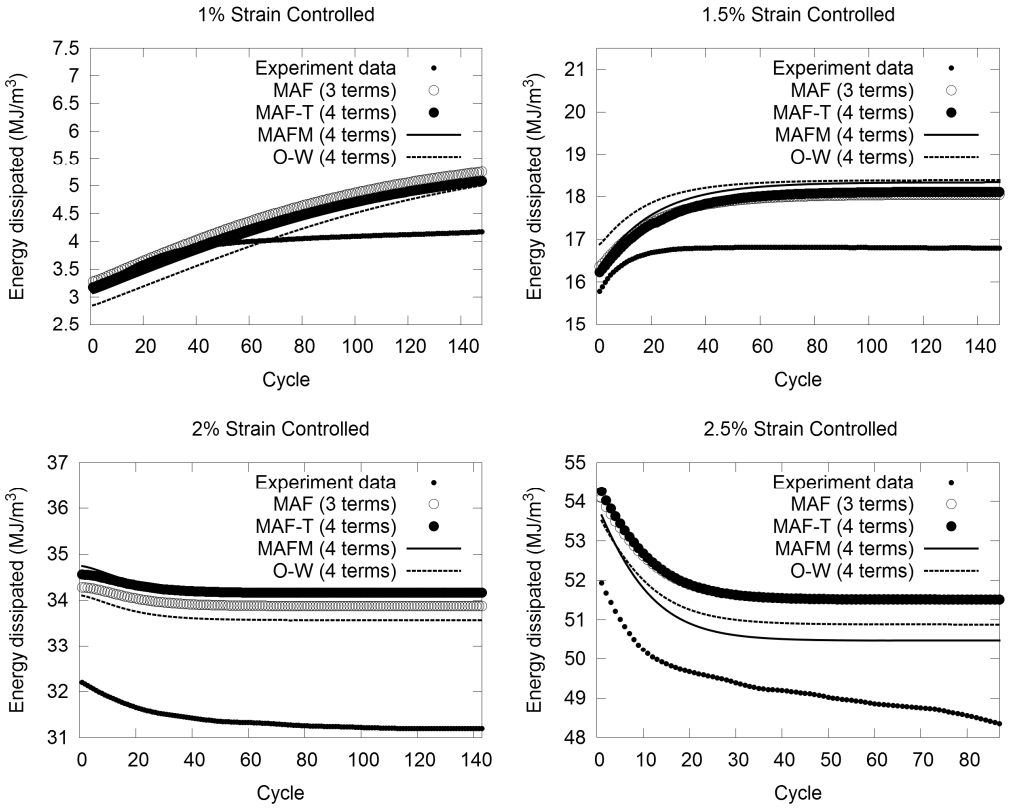

Figure 7. Plastic Strain Energy Density, per cycle, for experimental and simulated results.

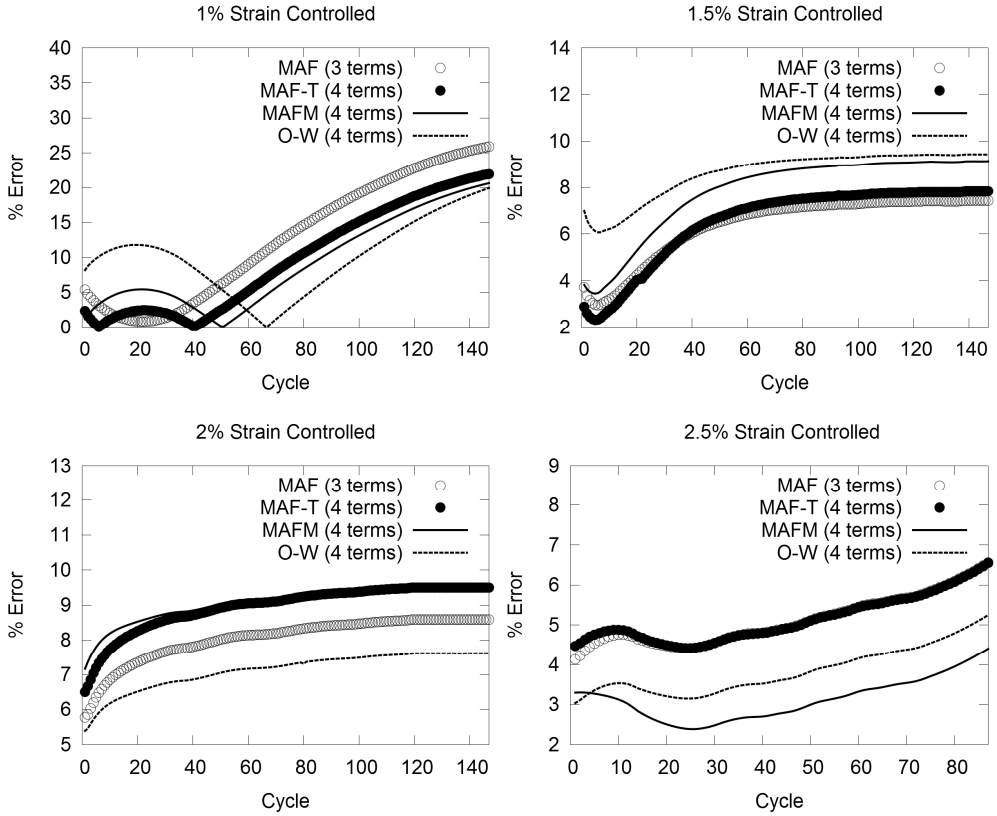

Figure 8. Plastic Strain Energy Density percentile error (%Error), per cycle, between experimental and computed results for each of the models compared.

5.2 Stress Controlled Results

The investigation of ratcheting behaviour (plastic strain accumulation under cyclic loading) of the SLM material (as-built Ti-6Al-4V) was a focal point for this research. Such results, experimental and computational, have not been reported so far, to the best knowledge of the authors, and were considered important for the completeness of this work. As mentioned, a set of different loading histories was utilised to obtain the ratcheting curves (as detailed in Table 2). Figure 9 presents the experimental and computational ratcheting results for each stress pair, while Figure 10 presents the percentile error (%Error) between computational and experimental results (for each of the models compared). One may notice that, again, the performance of the different models is varied, especially when observing the %Error curves. These findings are instrumental for the overall comparison and assessment of the plasticity models.

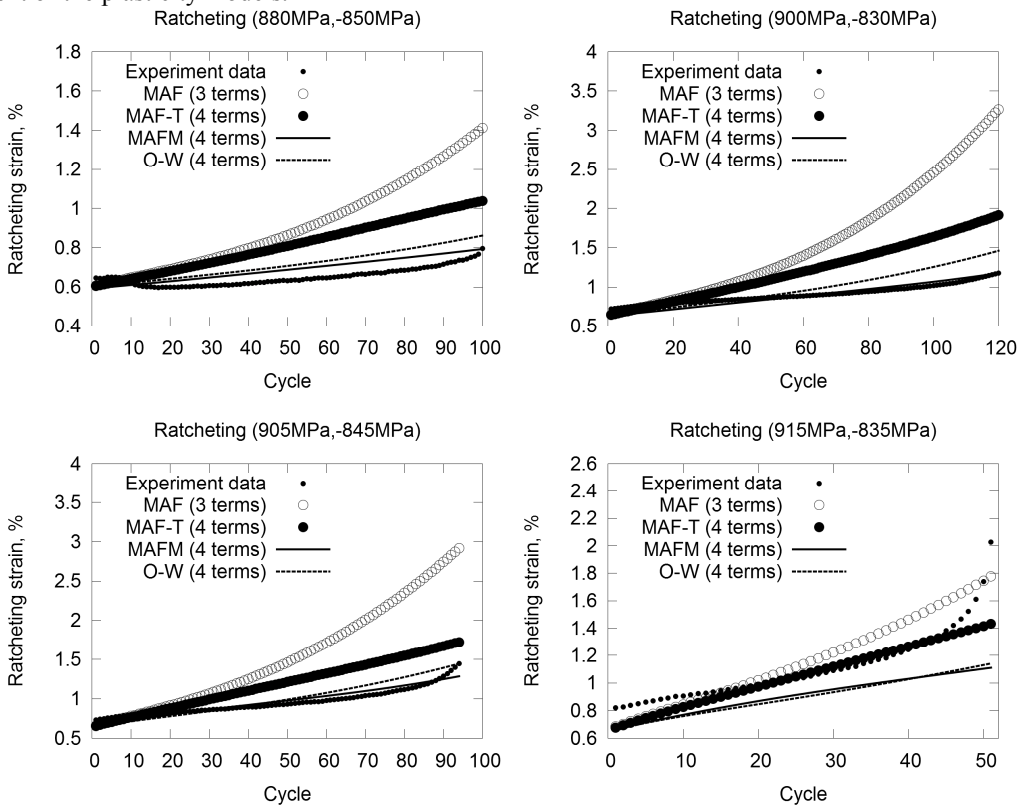

Figure 9. Ratcheting strain per cycle for each of the stress controlled loading cases for experiments and computed results, for each of the models compared.

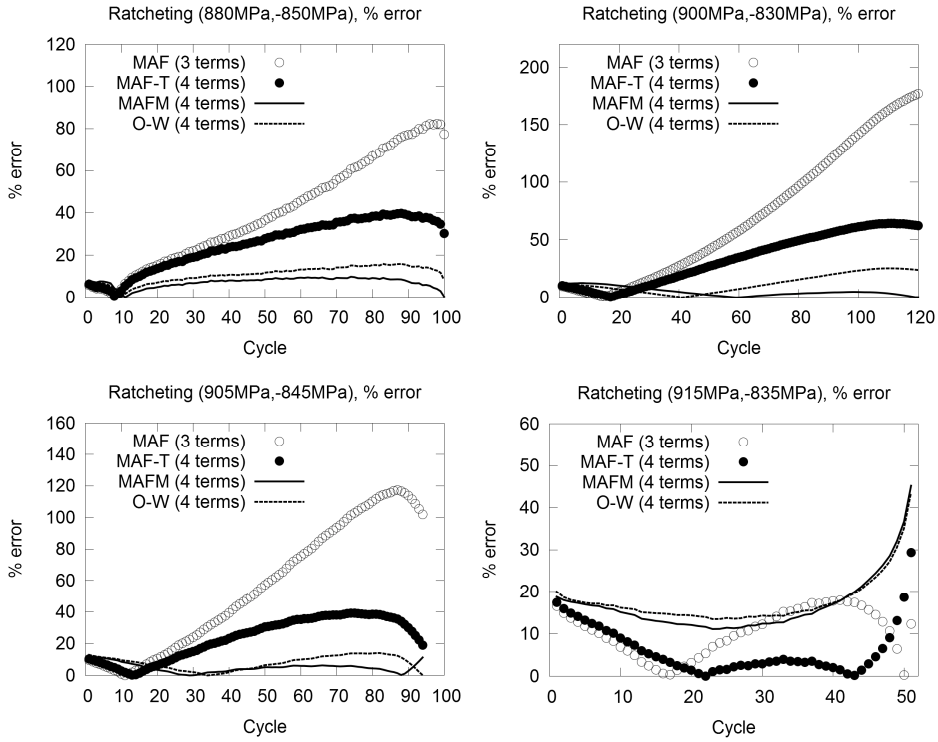

Figure 10. Ratcheting strain per cycle percentile error (%Error) between experimental and computed results for each of the models compared.

5.3 Overall Performance of the Models

The need for a simple way to conduct an overall comparison is apparent by examining the various results obtained, for both strain and stress controlled loading histories. The four plasticity models have proven to be, in general, capable to simulate effectively complex elastoplastic phenomena. However, when it comes to electing a model to be used in actual engineering applications it is not apparent or at least easily identifiable which would be the most suitable one. For the engineering practitioner such a decision would be done on the basis of a good trade-off between the different characteristics, advantages and disadvantages of each model. Effectively, a ranking scheme could be considered as a good tool to assist the decision making process. Such a ranking scheme is exemplified in this study.

The proposed scoring scheme relies on a weighting matrix which assigns different points at the various levels of percentile error (%error) achieved by each of the models. Lower performance (greater %Error) is assigned with lower points and the opposite. For simplicity, four different error levels and discrete point values were used for this example ranking scheme (Table 4).

3	Error < 5%
2	5% < Error < 10%
1	10% < Error < 20%
0	Error > 20%

Table 4. Weighting Matrix for scoring scheme

Employing the weighting matrix in all different cases leads to a scoring table for each of the models compared (MAF, MAF-T, MAFM and O-W). These results are presented in Table 5, where each model's performance is noted (in terms of the %error achieved). The different colours represent the number of points assigned for each case and when summed a total (overall) score results for each model (Table 6).

Model	Simulation Results																			
	Stress Controlled				Strain Controlled															
	Ratcheting Rate				Mean Stress Relaxation				Hysteresis Loop (1st Cycle)				Cyclic Hardening (H value)				Plastic Deformation Energy			
	Test 1	Test 2	Test 3	Test 4	Test 1	Test 2	Test 3	Test 4	Test 1	Test 2	Test 3	Test 4	Test 1	Test 2	Test 3	Test 4	Test 1	Test 2	Test 3	Test 4
MAF	40.0%	70.5%	55.7%	10.4%	6.2%	6.8%	0.8%	4.4%	9.5%	7.4%	14.9%	7.7%	71.8%	19.9%	1.4%	23.8%	10.8%	6.0%	7.9%	4.9%
MAFT	25.4%	34.1%	23.6%	6.1%	5.6%	6.3%	0.8%	7.7%	9.3%	6.6%	15.0%	7.9%	63.8%	20.5%	1.3%	27.6%	9.8%	6.6%	9.0%	5.1%
MAFM	7.3%	5.2%	5.0%	16.7%	5.1%	6.7%	1.0%	0.8%	8.9%	6.6%	18.1%	8.0%	63.0%	23.2%	3.9%	30.0%	5.7%	7.3%	9.0%	3.1%
O-W	11.0%	12.2%	8.0%	17.7%	4.4%	7.7%	0.8%	1.4%	9.3%	9.7%	15.9%	7.9%	65.3%	24.2%	3.1%	22.3%	12.8%	8.6%	7.1%	3.8%

Table 5. Score Matrix results for each model compared - Average Error% for each test case examined.

MAF	MAFT	MAFM	O-W
30	29	37	34

Table 6. Overall score for each model

The total (overall) score obtained for each model may be used as a descriptor of the overall performance of the model, in comparison to other models. From this example one may notice that the difference between models may be rather small (in terms of points collected), however some models do tend to perform better when examining their overall characteristics (e.g. MAFM and O-W, as compared to the simplest MAF and the widely used MAF-T). Of course, this scoring scheme is not the only applicable or the best available (in terms of accuracy) to conduct a representative comparison. This example intends primarily to highlight the importance of such (simple) scoring schemes for decision making processes. These can be particularly useful for engineering practitioners considering to employ advanced plasticity models, as opposed to built-in models in commercial finite element software (such as the rather simple MAF model).

6 Conclusions

This study aimed to identify the basic cyclic elastoplastic characteristics of as-built SLM Ti-6Al-4V and moreover assess the capability of constitute models to simulate this behaviour. The four models employed in this regards were successful in simulating complex phenomena arising from uniaxial strain and stress controlled loading histories. This research is one of the few investigations reported to date on SLM material. Phenomena associated with the fatigue performance of this class of metals can be captured with reasonable accuracy with this set of models, with some of the models being more promising (as indicated by this rough comparison). Engineering design considerations, especially for applications where high and low cycle fatigue is a critical operating factor, can benefit from these mechanical testing and simulation results. Moreover, these findings can be helpful as a basis and initiator for further studies on as-built SLM Ti-6Al-4V, for which very few published data exist.

Another interesting finding was that the cyclic plasticity models compared, quite widely used by industry and academia, have a varied performance under different loading cases and parameters. A scoring scheme, for the assessment of their overall performance, can be utilised for a quick and easy comparison. This can be especially useful for practicing engineers wishing to go beyond the classic MAF model or, its derivative, MAF-T model. A more sophisticated scoring scheme (e.g. utilising discrete and non-discrete values weighing matrices), as opposed to the example used, could lead to the development of a more comprehensive tool for researchers and engineers. This study has also provided the grounds for the MAFM model to confirm its value not only as an alternative to the MAF-T model but moreover as a versatile model capable to simulate the behaviour of various classes of metal alloys (Kourousis and Dafalias, 2013; Dafalias et al., 2008). However, a more detailed analysis and implementation of the MAFM model for other metal alloys, and in the multiaxial regime, is considered necessary for its further validation.

7 Acknowledgments

The support of the Centre for Advanced Manufacturing of RMIT University is acknowledged. Moreover, we would like to thank particularly Professor Milan Brandt and Dr Shoujin Sun, of RMIT University, for their assistance in matters related to SLM material characteristics and manufacturing process.

References

Armstrong, P.J.; Frederick, C.O.: A mathematical representation of the multiaxial Bauschinger effect. *G.E.G.B. Report RD/B/N,* 731 (1966)

Bari, S.; Hassan, T.: Anatomy of coupled constitutive models for ratcheting simulation. *Int. J. Plast.,* 16, (2000), 381-409.

Chaboche, J. L.;, Dang-Van, K.; Cordier, G.: Modelization of the strain memory effect on the cyclic hardening of 316 stainless steel. In: Fifth International Conference on SMiRT, Berlin, Germany (1979).

Chaboche, J.L.: On some modifications of kinematic hardening to improve the description of ratchetting effects. *Int. J. Plast.*, 7, (1991), 661-678.

Dafalias, Y.F.; Kourousis, K.I.; Saridis, G.J: Multiplicative AF kinematic hardening in plasticity. *Int. J. Sol. Struct.*, 45, (2008), 2861-80.

Huang, S.; Leary, M.; Ataalla, T.; Probst, K.; Subic, A.: Optimisation of Ni–Ti shape memory alloy response time by transient heat transfer analysis. *Mat. Des.*, 35, (2012), 655–663.

Kourousis, K.I.; Dafalias, Y.F.: Constitutive modeling of Aluminum Alloy 7050 cyclic mean stress relaxation and ratcheting. *Mech. Res. Comm.*, 53, (2013), 53-56.

Leary, M.; Maciej, M.; Lumley, R.; Subic, A.: An integrated case study of material selection, testing and optimization. In: Proceedings of the 17th International Conference on Engineering Design (ICED'09), 7, Stanford University, Palo Alto, CA, USA. (2009)

Leary, M.; Babaee, M.; Brandt, M.; Subic, A.: Feasible build orientations for self-supporting fused deposition manufacture: A novel approach to space-filling tesselated geometries. *Adv. Mat. Res.*, (2013a), 148-168.

Leary, M.; Shidid, D.; Mazur, M.; Brandt, M.; Subic, A.: Topographic optimization with variable boundary conditions: Enabling optimal design of interacting components, In: Proceedings of the International Conference on Engineering Design, ICED, 9, 23-30 (2013b).

Leuders, S.; Thone, M.; Riemer, A.; Niendorf, T.; Troster, T.; Richard, H.A.; Maiera, H.J.: On the mechanical behaviour of titanium alloy TiAl6V4 manufactured by selective laser melting: Fatigue resistance and crack growth performance. *Int. J. Fat.*, 48, (2013), 300-307.

Mayeur, J.R.; McDowell, D.L.; Neu, R.W.: Crystal plasticity simulations of fretting of Ti-6Al-4V in partial slip regime considering effects of texture. *Comp. Mat. Sci.*, 41, (2008), 356-365.

Ohno, N.; Wang, J.D.: Kinematic hardening rules with critical state of dynamic recovery, part I: formulation and basic features for ratchetting behaviour. *Int. J. Plast.*, 9, (1993a), 375-90.

Ohno, N.; Wang, J.D.: Kinematic hardening rules with critical state of dynamic recovery, part II: Application to experiments of ratchetting behavior. *Int. J. Plast.*, 9, (1993b), 391-403.

Phaiboonworachat, A.; Cyclic Elasto-plastic Behaviour of Additive Manufactured Metals, Final Year Project, RMIT University, Melbourne, Australia, (2014).

Simonelli, M.; Tse, Y.Y.; Tuck, C.: Further understanding of Ti-6Al-4V selective laser melting using texture analysis, In: 23rd Annual Int. Solid Freeform Fabrication Symp., 480, (2012).

Vrancken, B.; Thijs, L.; Kruth, J-P; Van Humbeeck, J.: Heat treatment of Ti6Al4V produced by Selective Laser Melting: Microstructure and mechanical properties. *J. Alloys Compd*, 541, (2012), 177-185.

Xu, W.; Sun, S; Elambasseril, J.; Liu, Q.; Brandt, M.; Qian, M.: Ti-6Al-4V additively manufactured by selective laser melting with superior mechanical properties. *JOM*, 67, (2015), 668-673.

Zhang, M.; Zhang, J.; McDowell, D.L.: Microstructure-based crystal plasticity modeling of cyclic deformation of Ti-6Al-4V. *Int. J. Plast.*, 23, (2007); 1328-1348.

Address: K. Kourousis, Department of Mechanical, Aeronautical and Biomedical Engineering, University of Limerick, Limerick, Ireland; School of Aerospace, Mechanical and Manufacturing Engineering, RMIT University, Melbourne, VIC, Australia
email: kyriakos.kourousis@ul.ie

D. Agius, School of Aerospace, Mechanical and Manufacturing Engineering, RMIT University, Melbourne, VIC, Australia

C. Wang, School of Aerospace, Mechanical and Manufacturing Engineering, RMIT University, Melbourne, VIC, Australia

A. Subic, School of Aerospace, Mechanical and Manufacturing Engineering, RMIT University, Melbourne, VIC, Australia